*Egypt. J. Chem.* **Vol. 66**, No. 7 pp. 245 - 256 (2023)

**Egyptian Journal of Chemistry**

**http://ejchem.journals.ekb.eg/**

# Investigating the Kinetic Parameters in the Thermal Analysis of Jojoba Cake

**N.M. Madany[1]*, M.A. Gadalla[2], F.H. Ashour[1] and M.F. Abadir[1]**

[1] *The chemical Engineering Department, Faculty of Engineering, Cairo University, Egypt*

[2] *The chemical Engineering Department, Faculty of Engineering, Port-Said University, Egypt*

**Abstract**

Jojoba seeds are processed to produce an oil of use in many industries. The cake left after oil extraction contains obnoxious substances which make it hazardous to use as animal fodder. In the present work, thermal analysis was used to identify the kinetics of biochar formation from the de-oiled residue. TG –DTG curves showed that decomposition takes place in two major steps corresponding to the devolatilization of hemicellulose, cellulose, and lignin. The residual material left consists of biochar which undergoes cracking up to about 500$^{o}$C. The final ash constitutes about 17.2% of the dry material. Three iso-conversional methods were used in that work to investigate the decomposition kinetics, namely the FWO, KSA and Friedman techniques. Results proved that while the first decomposition step followed first order kinetics with average activation energy values ranging from 86.19 to 90.11 kJ.mol$^{-1}$, the second step was controlled by reaction at interface with activation energies ranging from 93.26 to 99.37 kJ.mol$^{-1}$, depending on the kinetic model used.

Keywords: Jojoba; De-oiled cake; Thermal analysis; Kinetics; Activation energy

## 1. Introduction

Jojoba (*Simmondsia chinensis*) is an industrial crop plant, cultivated for its seed, from which a highly valuable oil is obtained[1]. Jojoba oil is used in diverse applications such as cosmetic, pharmaceutical, lubricant, heating insulator, foam control agent, high-pressure lubricant, heating oil, plasticizer, fire retardant, transformer oils and many more[2,3].Jojoba oil is normally extracted from its seeds through mechanical pressing, the de-oiled cake usually containing from 3 to 8% of oil that cannot be extracted mechanically[3]The main oily product of jojoba is a liquid wax composed mainly of straight chain monoesters in the range of C40–C44 [4]while the remaining meal is rich in protein [2,5]. The protein content in the meal varies between 26 and 33% making it attractive as a livestock feed. Unfortunately, about 15% of this meal is constituted of a group of toxic glycosides making it hazardous to use as animal fodder[5,6,7].The presence of antinutritional factors in jojoba cake [8], such as simmondsin, simmondsin-2-ferulate, phenol, and phytic acid decrease food intake, body weight, affect biochemical parameters, and deteriorate animal fertility [2,8,9].

The preparation and characterization of biochar from jojoba feedstock has been researched by Zhang et al [10]who determined the proximate analysis, basic chemical elements content, BET surface area and FTIR of the feedstock. They also showed using thermal analysis that the formation of biochar was completed at 600$^{o}$C after devolatilization of hemicellulose, cellulose and lignin at lower temperatures. The slight weight loss observed up to 800$^{o}$C was speculated to be due to the formation of highly aromatic microstructures above 600$^{o}$C, following the findings of Cui et al[11]. However, these authors did not discuss the kinetics of formation of biochar, or the associated steps observed during pyrolysis.

Although no detailed kinetics was reported for the pyrolysis of jojoba seeds or de-oiled cake, there has been some research connected with most vegetable waste. The activation energy of the different steps of pyrolysis and occasionally the mechanism of these reaction have been disclosed in studying the kinetics of pyrolysis of orange peels [12], banana peels [13],

*Corresponding author e-mail: neama.madany.a@eng-st.cu.edu.eg

EJCHEM use only: 05 September 2022; 27 September 2022; 05 October 2022

DOI: 10.21608/EJCHEM.2022.160576.6924

corncobs [14], bagasse and wheat straw [15] and similar species. However, no results have been reported so far for the kinetics of pyrolysis of jojoba seeds or de-oiled cake although kinetic studies have been carried out for a similar non-edible plant like jatropha. A detailed study for the pyrolysis of jatropha seeds was carried out by Tsekos et al [16] and Saiid et al [17] while the kinetics of pyrolysis of jatropha de-oiled cake was researched by Sharma et al [18].

In the present work, it was proposed to use de-oiled jojoba seeds cake (DOJC) in the preparation of biochar through a pyrolysis process. The necessary conditions to obtain that char are determined by investigating the kinetics of its formation. This is actually the main purpose of the present work which also aims at disclosing the kinetic mechanism associated with biochar formation and the activation energy required for that process.

## 2. Experimental Techniques

In the present work, de-oiled jojoba cake (DOJC) - used as biomass - was collected from Cleopatra Company for natural oil production, El-Fayoum, Egypt, in a form of solid pellets. DOJC was oven dried overnight at 105°C, then hand ground to pass 100 mesh sieves (150µm). The dried powder was then identified by FTIR using Class1 Laser Product IEC/EN 60825-1/A2:2001 Avatar Series (USA).

### *2.1. Calorific value*

The calorific value is the heat produced by the complete combustion of a specified quantity of the material (Here, 1784 mg of DOJC). This was determined using a Parr 6200 bomb calorimeter.

### *2.2. Thermal analysis:*

20 mg of the powder was then heated in a thermal analyzer (Universal V4.5A TA Instruments) in nitrogen flow at 50 mL.min-1 to produce TGA and DTG traces at four different heating rates: 5, 10, 15 and 20°C.min-1. After assessing the temperature at which biochar is formed, 10 g of collected DOJC were heated in a muffle furnace in which nitrogen was flown at 10°C.min-1 to that temperature. After the mass was left to cool, its chemical constitution was determined by EDX analysis using EDX-LE Shimadzu analyzer. This step was repeated at a higher temperature to assess the change in char composition following cracking.

### *2.3. Determination of the percent of lignocellulosic components*

The determination of the percent lignocellulosic components (Hemicellulose – cellulose and lignin) in DOJC was carried out following the methods described by Jin et al [19] which relied on the early work of Van Soest et al [20] and Collings et al [21].

- Determination of Cellulose

The cellulose percent was determined by dissolving the powder in sodium sulfite then sodium chlorite to remove hemicellulose and lignin. The remaining residue is fired to 600oC and the percent loss in weight on firing represents the percent cellulose in the sample.

- Determination of Hemicellulose:

The hemicellulose present was determined by heating to 80oC in acetic acid and sodium chlorite. The suspension is then removed to another beaker where sodium hydroxide is added at 80oC to complete the dissolution of cellulose. After filtration, the cake is dried, weighed and fired at 600oC. The percent loss in weight on firing represents the percent hemicellulose.

- Determination of Lignin:

The lignin percent was determined by dispersing the powder in ammonium oxalate, boiling and filtering. The solid cake was suspended in 1% acetic acid at 70°C and sodium chlorite and acetic acid were added to oxidize lignin. The suspension was then filtered and dried at 60°C for 4h. The difference in weight represents the lignin percent.

## 3. Kinetic calculations

Three different methods were used to disclose the kinetics of pyrolysis using the TGA traces obtained at the different heating rates. In general, these methods rely on determining the conversion (α) following any weight loss using the expression:

$$\alpha = \frac{m - m_f}{m_0 - m_f} \qquad (1)$$

Where, $m$ : is the mass remaining in general after any time during weight loss.

$m_0$ : is the initial mass.

$m_f$ : is the final mass at the termination of the weight loss step.

The general kinetic equation upon which all different calculation techniques are based takes the following form where the rate of reaction is represented by (dα/dt):

$$\frac{d\alpha}{dt} = Ae^{-\frac{E}{RT}}.f(\alpha) \qquad (2)$$

Where, $E$: is the activation energy J.mol$^{-1}$, required to be determined.

$R$ : is the general gas constant = 8.314 J.mol$^{-1}$.K$^{-1}$.

$A$ : is the pre-exponential factor.

This equation can be integrated after separating variables to give:

$$\int \frac{d\alpha}{f(\alpha)} = g(\alpha) = \int A e^{-\frac{E}{RT}}.dt \qquad (3)$$

Under isothermal conditions, it takes the final form:

$$g(\alpha) = k.t = A e^{-\frac{E}{RT}}.t \qquad (4)$$

**Table 1**
Different forms of the kinetic functions f(α), g(α)[20]

| Code | Controlling step | $f(\alpha)$ | $g(\alpha)$ |
|---|---|---|---|
| A | Crystallization and grain growth | $2(1-\alpha).[\ln(1-\alpha)]^{\frac{m-1}{m}}$ | $[-\ln(1-\alpha)]^{1/m}$ |
| F0 | Zero order reaction | 0 | $\alpha$ |
| F1 | First order reaction | $1-\alpha$ | $-\ln(1-\alpha)$ |
| Fn | *n*th order reaction ($n \neq 1$) | $(1-\alpha)^n$ | $\frac{(1-\alpha)^{1-n}}{1-n}$ |
| R2 | Cylindrical: reaction at interface | $2(1-\alpha)^{\frac{1}{2}}$ | $1-(1-\alpha)^{\frac{1}{2}}$ |
| R3 | Spherical: Surface reaction at interface | $3(1-\alpha)^{\frac{2}{3}}$ | $1-(1-\alpha)^{\frac{1}{3}}$ |
| D1 | One dimensional diffusion | $\frac{1}{2\alpha}$ | $\alpha^2$ |
| D2 | Two-dimensional diffusion | $-\ln(1-\alpha)$ | $\alpha + (1-\alpha).\ln(1-\alpha)$ |
| D3 | Three-dimensional diffusion (Thin ash layer) | $\frac{3(1-\alpha)^{\frac{2}{3}}}{2-(1-\alpha)^{\frac{1}{3}}}$ | $\left[1-(1-\alpha)^{\frac{1}{3}}\right]^2$ |
| D4 | Spherical: diffusion through ash | $\frac{1}{2\left[(1-\alpha)^{-\frac{1}{3}}-1\right]}$ | $1-\frac{2}{3}\alpha-(1-\alpha)^{\frac{2}{3}}$ |

The functions $f(\alpha)$ and $g(\alpha)$ depend on the mechanism involved in the reaction. A compilation of the most probable mechanisms has been reported by Khawam et al [22]. These are shown in Table (1).

In the present work, three iso-conversional methods were used from which the activation energy could be determined without indicating the mechanism of reaction.

The first method, known as the Flynn – Wall – Ozawa (FWO) relies on determining the activation energy from the following expression [23]:

$$log\,\beta = ln\frac{A.f(\alpha)}{\frac{d\alpha}{dT}} - 0.456\frac{E}{RT} \qquad (5)$$

Where, : is the heating rate $^{o}$C.min$^{-1}$.

Hence a plot of $\log\beta$ against $\frac{1}{T}$ for fixed values of conversion $(\alpha)$should produce a straight line of slope $= -\frac{0.456\,E}{R}$

The second method, known as the Kissinger – Akahira – Sunose (KAS) method [24] uses the following expression to calculate activation energy:

$$ln\frac{\beta}{T^2} = -\frac{E}{RT} + ln\frac{R.A(\alpha)}{E.g(\alpha)} \qquad (6)$$

At fixed values of conversion, a plot of ln $\frac{\beta}{T^2}$ against *(1/T)* will yield straight lines of slope $= -E/R$ .

The third method, elaborated by Friedman [25] relies on rewriting equation (2) in the form:

$$\frac{d\alpha}{dt} = \frac{d\alpha}{dT}.\frac{dT}{dt} = \beta\frac{d\alpha}{dT} = A e^{-\frac{E}{RT}}.f(\alpha) \qquad (7)$$

$$ln\,\beta\frac{d\alpha}{dT} = ln\,A.f(\alpha) - \frac{E}{RT} \qquad (8)$$

Therefore, a plot of $\ln\beta\frac{d\alpha}{dT}$ vs $(1/T)$ at different values of conversion $(\alpha)$ should produce a series of straight lines of slope $= -\frac{E}{R}$ and intercept $\ln A.f(\alpha)$. It is possible to determine the values of $\ln A$ for the different conversion levels if the expression of $f(\alpha)$ is known. This can be obtained from Table (1) following a reasonable assumption for the rate controlling step. According to the kinetic compensation principle [26], a plot between the values of $\ln A$ and those of $E$ obtained at different values of $\alpha$ should produce a straight line. Obtaining a linear relation in the following form helps validating the proper choice of $f(\alpha)$ and hence the controlling mechanism:

$$ln\,A = a + b.E \qquad (9)$$

## 4. Results and Discussion

### *4.1. Characterization of raw material (DOJC)*

- FTIR analysis of DOJC)

Figure (1) shows the FTIR pattern obtained on subjecting the dried DOJC powder to IR analysis. Table (2) indicates the nature of the peaks obtained.

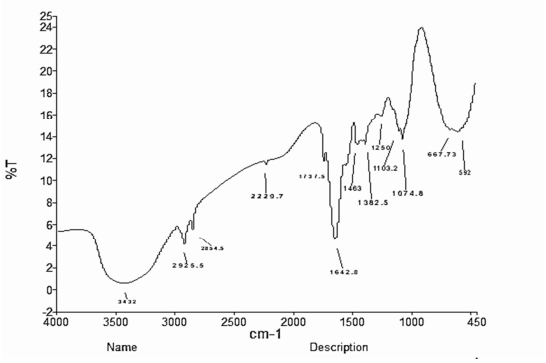


**Fig 1:** FTIR pattern of DOJC

**Table 2**
Main functional groups bands from FTIR of DOJC [27]

| Peak # | Wave number cm-1 | Band origin |
|---|---|---|
| 1 | 3432 | – OH |
| 2 | 2925 | – CH2 and – CH3 |
| 3 | 2854 | C–H |
| 4 | 2230 | C≡N |
| 5 | 1738 | C=O |
| 6 | 1643 | C=O |
| 7 | 1463 | C=C |
| 8 | 1383 | C–H |
| 9 | 1250 | C-O |
| 10 | 1103 | C-O |
| 11 | 1075 | C-O |
| 12 | 668 | C-H bending out of plane |
| 13 | 592 | C-O |

- Calorific value of DOJC

A high figure was obtained for the net calorific value of DOJC namely,21990 kJ.kg$^{-1}$, as determined using the bomb calorimeter (Section 2.1). One possible reason is the remnant oil fraction in the seed residue. This elevated figure sets the cake residue as potential waste derived fuel to be used in industrial furnaces partially replacing conventional fossil fuels provided an oxidizing atmosphere prevails [28]. This value is much higher than that reported by Al-Hamamre et al [29] who gave a value of 15340 kJ.kg$^{-1}$. One reason for the discrepancy could be the difference in residual oil content in the two cases. In the present case, a lab test performed by dissolving 100 g of the dry powder in hexane following a similar work by Warra et al [30]. It was found to equal about 7 % by weight of the dry powder.

- Determination of the lignocellulosic components of DOJC

The percentages of lignocellulosic components in the waste investigated were determined by the methods described by Jin et al [19]. The following results were obtained Table (3).

**Table 3**
Lignocellulosic components in DOJC

| Component | Cellulose | Hemicellulose | Lignin |
|---|---|---|---|
| | Weight % | | |
| Sample # 1 | 28.68 | 9.36 | 8.35 |
| Sample # 2 | 27.36 | 9.18 | 9.12 |
| Average | 28.02 | 9.27 | 8.735 |

The above table suggests that the total percentage of lignocellulosic materials amounts to about 46% of the dry mass.

### *4.2. Thermal analysis*

TGA and DTG curves were obtained for DOJC in nitrogen flow at the four aforementioned heating rates. The pattern obtained was similar for all heating rates except that the peak temperatures increased with increasing heating rates. Fig (2) illustrates the pattern obtained at a heating rate of 10°C.min$^{-1}$.

An initial weight drop ending at about 200°C corresponds to the loss of humidity and amounts to about 9% of the original mass. Two DTG peaks follow: A first peak at 249.3°C and a second one at 346.15°C. The first peak corresponds to a loss in weight starting at about 200°C and ending at about 270°C. According to Zhang et al [10], this step corresponds to the devolatilization of hemicellulose and partially cellulose and lignin. The following step starts at about 270°C and ends at about 380°C and corresponds to the final decomposition of lignin. At that temperature, biochar is formed and further loss in weight can be attributed to cracking of the formed

biochar which was observed during the pyrolysis of several types of biomass [28]. The total loss in weight following the second step constitutes about 51% of the dry mass, a figure almost compatible with the total percent of lignocellulosic materials as per the results of Table (3).

The loss in weight almost stabilized above 500°C.The final remaining residue at 900°C consisted of ash constituting about 16.09% of the dry mass.

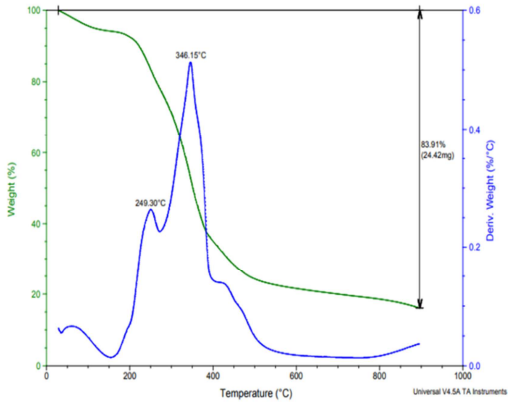


**Fig 2:** TGA – DTG curves for DOJC at heating rate = 10°C.min$^{-1}$

*4.3. Kinetics of the first decomposition step*

- Conversion curves

Table (4) reveals the initial and final temperatures of the first decomposition step at the four heating rates together with the maximum peak temperature in each case. Figure (3) illustrates the conversion as function of temperature for different heating rates, as calculated from equation (1).

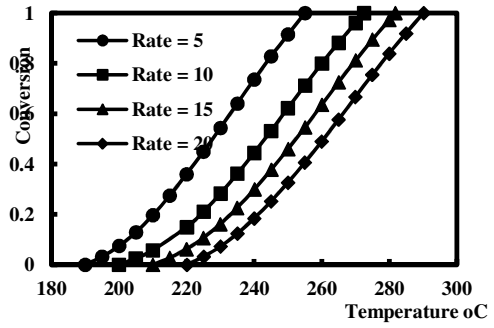


**Fig 3:** Conversion as function of temperature at different heating rates (First step)

**Table 4**
Characteristic temperatures for the first decomposition step

| Heating rate $\beta$°C.min-1 | 5 | 10 | 15 | 20 |
|---|---|---|---|---|
| Beginning temperature oC | 190 | 200 | 210 | 220 |
| Peak temperature °C | 232 | 250 | 258 | 268.5 |
| Final temperature °C | 255 | 270 | 282 | 291 |

- Results using the FWO method

As previously described, this method relies on plotting $\log \beta$ against $(1/T)$ for fixed values of conversions. Figure (4) illustrates these plots for values of $\alpha$ ranging from 0.2 to 0.8. The straight lines obtained are almost parallel and the values of activation energy obtained from their slopes are summarized in Table (5). The average value of $E$ = 90.11 kJ.mol$^{-1}$.

**Table 5**
**Activation energy of the first decomposition step using the FWO method**

| α | 0.2 | 0.3 | 0.4 | 0.5 | 0.6 | 0.7 | 0.8 |
|---|---|---|---|---|---|---|---|
| E | 88.87 | 89.08 | 89.26 | 89.79 | 90.43 | 91.27 | 92.09 |
| $R^2$ | 0.9997 | 0.999 | 0.999 | 0.999 | 0.999 | 0.999 | 0.999 |

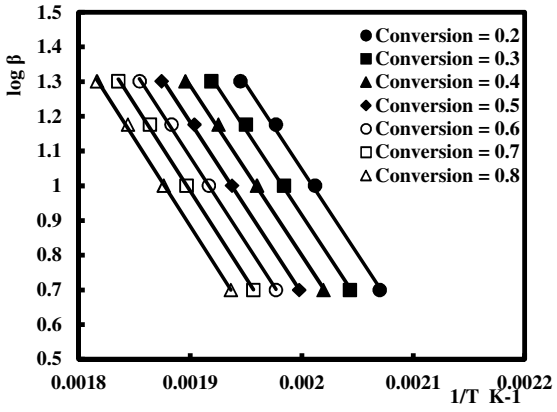


**Fig 4:** FWO plots for the first decomposition step

- Results using the KAS method

The plots of $ln(\beta/T^2)$ against $(1/T)$ at values of $\alpha$ ranging from 0.2 to 0.8 are illustrated in Figure (5). The straight lines obtained have sensibly equal slopes from which the values of activation energy shown in Table (6) were obtained.

**Table 6**
Activation energy of the first decomposition step using the KAS method

| α | 0.2 | 0.3 | 0.4 | 0.5 | 0.6 | 0.7 | 0.8 |
|---|---|---|---|---|---|---|---|
| E | 85.17 | 85.29 | 85.38 | 85.84 | 86.42 | 87.22 | 87.98 |
| R2 | 0.996 | 0.997 | 0.998 | 0.999 | 0.999 | 0.999 | 0.999 |

The mean value of activation energy = 86.19 kJ.mol$^{-1}$, a value close to that obtained using the FWO method.

A common feature that can be deduced from Table (5) and (6) is the fact that the values of activation energy increase with increased conversion as illustrated in Figure (6).

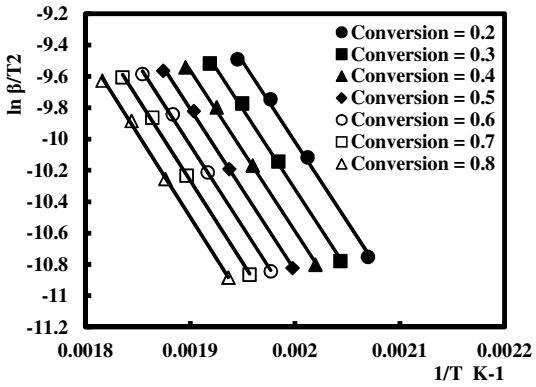


**Fig 5:** KAS plots for the first decomposition step

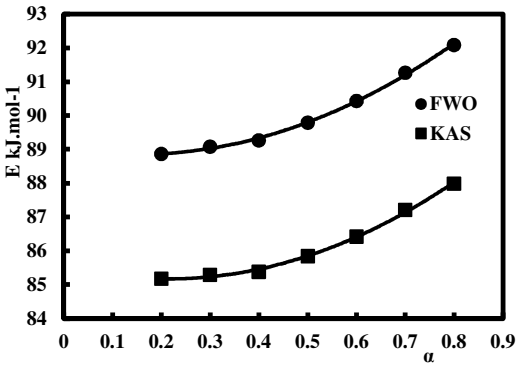


**Fig 6:** Variation of activation energy with conversion for the first decomposition step

- Results using the Friedman method

This method relies on plotting $\ln \beta.\frac{d\alpha}{dT}$ vs $(1/T)$ for different values of conversion $(\alpha)$. The slopes of these lines allow calculating the value of $E$ at each conversion level, while the intercepts produce values of $\ln A.f(\alpha)$. Figure (7) illustrates the straight lines obtained from which it was possible to deduce the values of $E$ reported in Table 7 with an average value = 88.62 kJ.mol$^{-1}$, a value matching those calculated by the FWO and KAS methods. Figure (8) shows that the values of $E$ generally increase with conversion except for a slight decrease at early conversion levels. The explanation of that deviation has to do with the approximation of $(d\alpha/dT)$ by $(\Delta\alpha/\Delta T)$ on applying Friedman method. In the present work, $\Delta\alpha$ was taken as 0.025, as recommended by all previous works used Friedman method. This is particularly true in the earlier stages of conversion (α < 0.4) where the curvature of the conversion-temperature curves is highest.

To obtain the values of $\ln A$, it was necessary to assume a controlling step for the decomposition step. In the present case, a first order reaction mechanism was assumed so that the expression of $f(\alpha)$ takes the form:

$$f(\alpha) = 1 - \alpha \qquad \textit{Table (1)}$$

The values of $\ln A$ are also shown in Table (7) and Figure (9) displays the linear relation between $\ln A$ and $E$. the elevated value of $R^2$ for that relation confirms the validity of the assumed form of $f(\alpha)$ and hence the first order reaction mechanism.Actually, the first order nature of the decomposition kinetics of hemicellulose and cellulose has been reported by several authors during pyrolysis of biomass [31-33].

**Table 7**
Activation energy of the first decomposition step using Friedman method

| α | 0.2 | 0.3 | 0.4 | 0.5 | 0.6 | 0.7 | 0.8 |
|---|---|---|---|---|---|---|---|
| E | 87.33 | 86.73 | 86.22 | 88.14 | 89.37 | 91.03 | 91.56 |
| R2 | 0.997 | 0.999 | 0.988 | 0.999 | 0.999 | 0.999 | 0.999 |
| ln *A* | 19.26 | 19.15 | 18.98 | 19.48 | 19.82 | 20.28 | 20.55 |

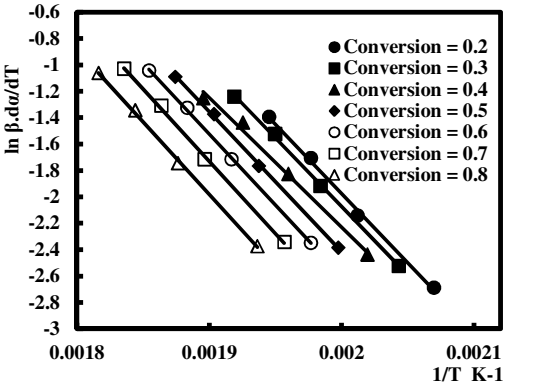


**Fig 7:** Friedman plots for the first decomposition step

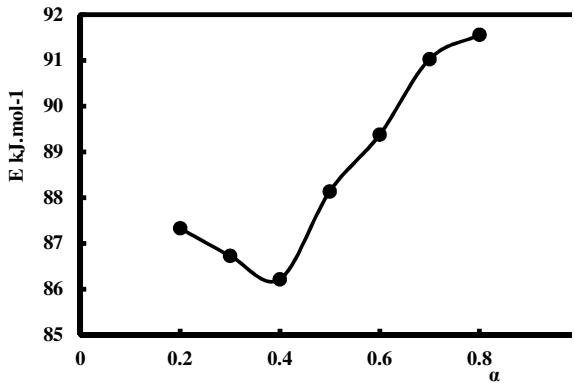


**Fig 8:** Variation of activation energy with conversion for the first decomposition step (Friedman method)

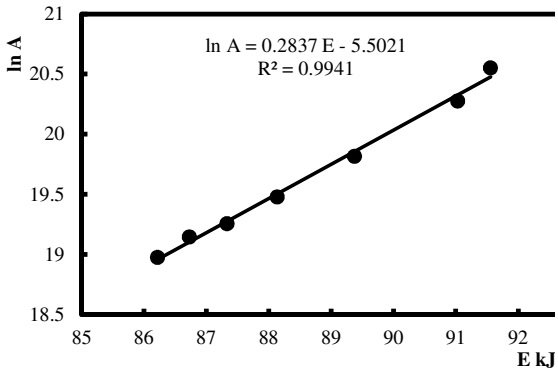


**Fig 9:** Linear relation between $\ln A$ and $E$ for the first decomposition step

*4.4. Kinetics of the second decomposition step*

- Conversion curves

The characteristic temperatures for the second decomposition step of DOJC are shown in Table (8) for the different heating rates. On the other hand, Figure (10) illustrates the dependence of conversion (as calculated from equation 1) on temperature on varying heating rates.

**Table 8**
Characteristic temperatures for the second decomposition step

| Heating rate $\beta$oC.min$^{-1}$ | 5 | 10 | 15 | 20 |
|---|---|---|---|---|
| Beginning temperature °C | 255 | 272 | 281 | 290 |
| Peak temperature °C | 327 | 346 | 352 | 366 |
| Final temperature °C | 340 | 370 | 390 | 405 |

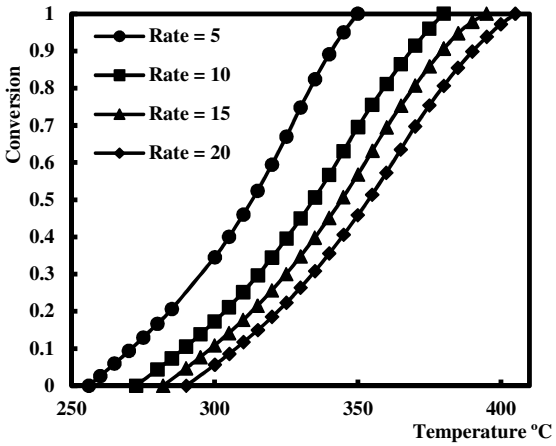


**Fig 10:** Conversion as function of temperature at different heating rates (Second step)

- Results using the FWO method

When values of $\log\beta$ were plotted against $\frac{1}{T}$ for values of conversions ranging from 0.2 to 0.8, the straight lines appearing in Figure (11) were obtained. The values of activation energy calculated from their slopes are summarized in Table (9) with an average value of $E$ = 99.37 kJ.mol$^{-1}$.

**Table 9**
**Activation energy of the second decomposition step using the FWO method**

| α | 0.2 | 0.3 | 0.4 | 0.5 | 0.6 | 0.7 | 0.8 |
|---|---|---|---|---|---|---|---|
| E | 97.0 | 98.55 | 99.92 | 99.84 | 99.53 | 98.20 | 94.57 |
| R2 | 0.998 | 0.998 | 0.998 | 0.997 | 0.996 | 0.995 | 0.993 |

- Results using the KAS method

Figure (12) shows the plots of ln $\frac{\beta}{T^2}$ against $\frac{1}{T}$, at values of $\alpha$ ranging from 0.2 to 0.8. The values of activation energy at the different levels of conversion are reported in Table (10).

**Table 10**
Activation energy of the second decomposition step using the KAS method

| α | 0.2 | 0.3 | 0.4 | 0.5 | 0.6 | 0.7 | 0.8 |
|---|---|---|---|---|---|---|---|
| E | 92.44 | 93.88 | 95.16 | 94.93 | 94.47 | 92.95 | 89.02 |
| R2 | 0.998 | 0.997 | 0.997 | 0.996 | 0.996 | 0.994 | 0.991 |

The mean value of activation energy = 93.26 kJ.mol$^{-1}$, a value close to that obtained using the FWO method. In both cases, the values of E start increasing with conversion to reach a maximum value at $\alpha \approx 0.45$ after which they go on decreasing. (Figure (13)).

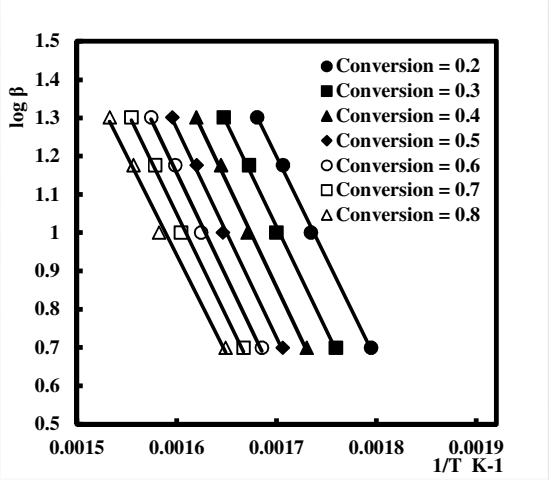


**Fig 11:** FWO plots for the second decomposition step

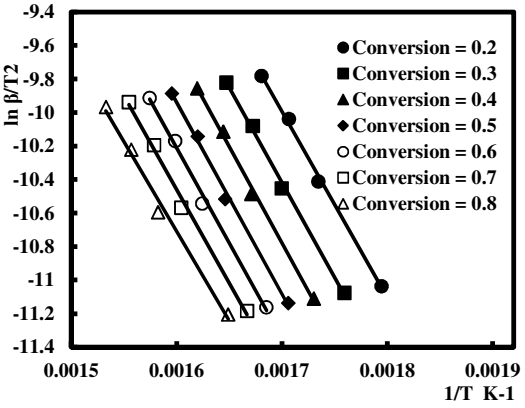


**Fig 12:** KAS plots for the second decomposition step

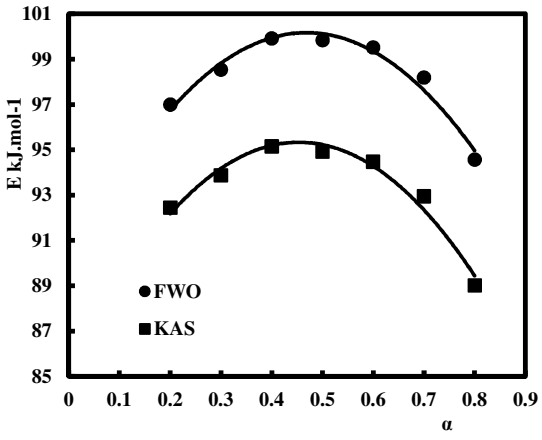


**Fig 13:** Variation of activation energy with conversion for the second decomposition step

- Results using the Friedman method

The same previously explained steps were carried out to obtain activation energy values as function of conversion from $\ln \beta \frac{d\alpha}{dT}$ vs $1/T$ plots (Figure (14)). The average value of $E = 93.69$ kJ.mol$^{-1}$coinciding with that obtained using the KAS technique Table (11). Activation energies go through a maximum value at $\alpha \approx 0.3$ (Figure (15)) and when a reaction at the interface between reacted core and unreacted ash was assumed, the calculated values of $\ln A$ varied linearly with $E$ (Figure (16)). Again, the elevated value of $R^2$ proved the validity of the chosen expression of $f(\alpha) = 3(1-\alpha)^{\frac{2}{3}}$, typical of a decomposition controlled by reaction at interface between core and product layer Table (1).

**Table 11**
Activation energy of the second decomposition step using Friedman method

| α | 0.2 | 0.3 | 0.4 | 0.5 | 0.6 | 0.7 | 0.8 |
|---|---|---|---|---|---|---|---|
| E | 96.9 | 102.7 | 99.58 | 94.86 | 91.98 | 86.55 | 83.15 |
| $R^2$ | 0.995 | 0.998 | 0.994 | 0.993 | 0.992 | 0.996 | 0.994 |
| ln *A* | 17.12 | 18.17 | 17.44 | 16.44 | 15.88 | 14.87 | 14.14 |

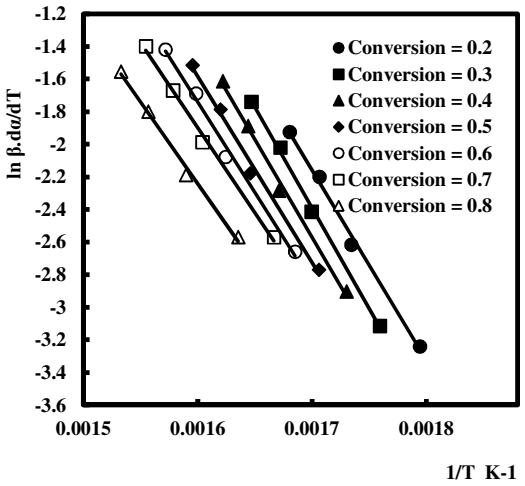


**Fig 14:** Friedman plots for the second decomposition step

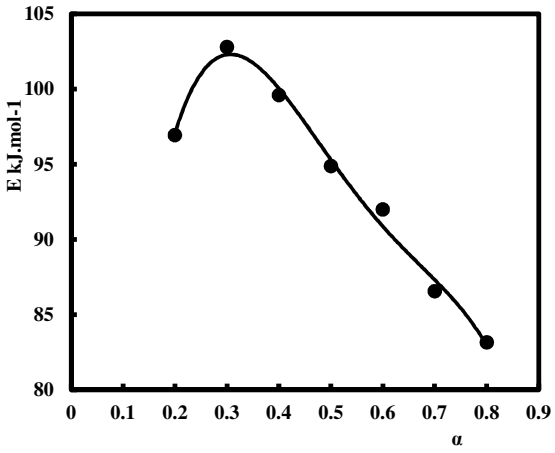


**Fig 15: Variation of activation energy with conversion for the second decomposition step (Friedman method)**

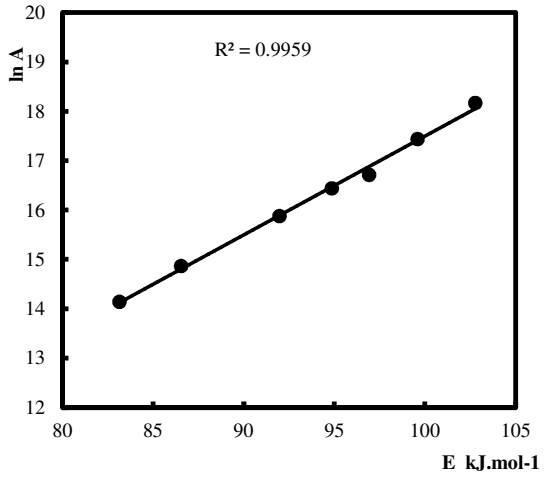


**Fig 16: Linear relation between ln $A$ and $E$ for the second decomposition step**

*4.5. Formation of biochar*

- Chemical composition of biochar

Figure (17) reveals the EDX pattern of biochar prepared at 400°C in which the carbon content is 76.41% while the corresponding SEM micrograph shows relatively low porosity as in Figure (18).

On the other hand, the EDX pattern for the specimen heated to 500°C, shows a lower carbon content (67.89%) as clear from Figure (19) as well as higher porosity as evidenced from the SEM micrograph in Figure (20). This is presumably due to the loss of some low molecular weight components on cracking. A similar result has been obtained by Li et al [34] who showed that an increase in pyrolysis temperature resulted in an increase in porosity. It appears that the cracking process of biochar has had for effect to eliminate the volatile fractions of low C content, resulting in a lower level of C remaining at 500°C compared to that present at 400°C.

**Fig 17**: EDX pattern of biochar prepared at 400°C

| Element | Weight% | Atomic% |
|---|---|---|
| C K | 76.41 | 82.03 |
| O K | 21.14 | 17.04 |
| Mg K | 0.29 | 0.15 |
| P K | 0.47 | 0.19 |
| S K | 0.10 | 0.04 |
| Cl K | 0.35 | 0.13 |
| K K | 1.08 | 0.36 |
| Ca K | 0.16 | 0.05 |
| Totals | 100.00 | |

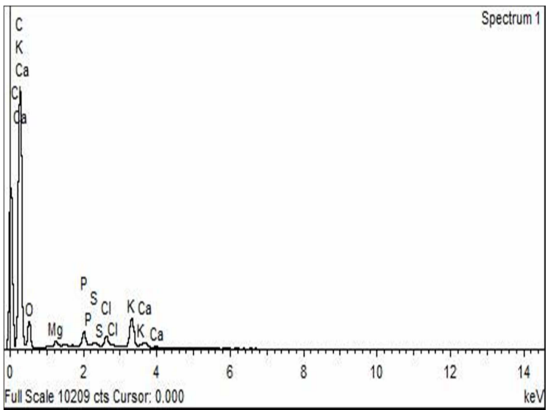

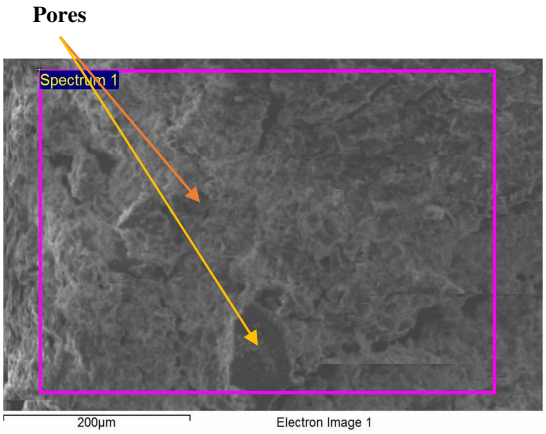


**Fig 18:** SEM micrograph of biochar prepared at 400°C

| Element | Weight% | Atomic% |
|---|---|---|
| C K | 67.89 | 74.13 |
| O K | 31.06 | 25.46 |
| Mg K | 0.17 | 0.09 |
| P K | 0.16 | 0.07 |
| S K | 0.07 | 0.03 |
| Cl K | 0.14 | 0.05 |
| K K | 0.40 | 0.13 |
| Ca K | 0.11 | 0.04 |
| Totals | 100.00 | |

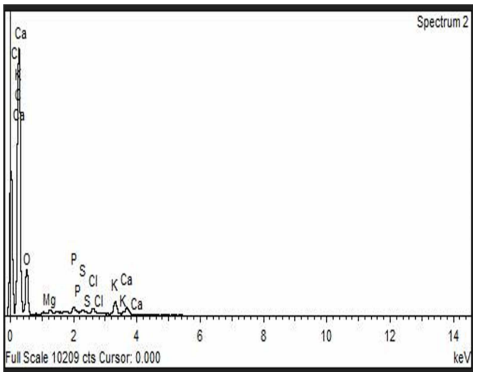


**Fig 19:** EDX pattern of biochar prepared at 500°C

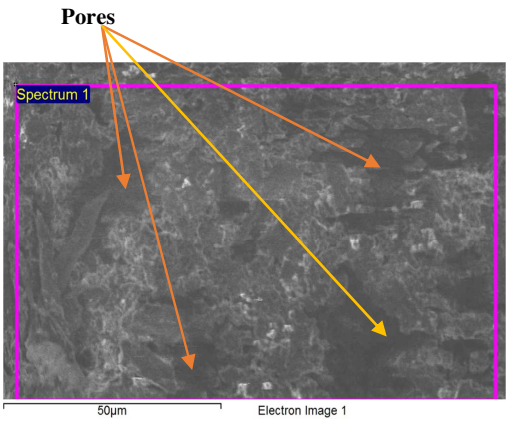


**Fig 20:** SEM micrograph of biochar prepared at 500°C

- Calorific value of biochar

The net calorific value of the biochar obtained at 400oC was determined and found to equal 27570kJ.kg-1, a value higher much than the value 17600kJ.kg-1 obtained by Mierzwa-Hersztek et al for coniferous tree bark biochar [35] and comparable to the value determined for biochar derived from mahogany wood chips pyrolyzed at a heating rate of 10°C.min-1 (26551 kJ.kg-1) [36]. The determined calorific value designates the investigated jojoba biochar as an excellent candidate for use as fuel.

## 5. Conclusion

The thermal analysis of jojoba de-oiled seeds in nitrogen showed two main decomposition steps ending by the formation of biochar at temperatures in the range of 400°C depending on the heating rate. The formed char underwent cracking up to about 500°C. The first decomposition step corresponding to the devolatilization of hemicellulose, cellulose and lignin was found to follow first order kinetics with an activation energy in the range 86.19 to 90.11 kJ.mol$^{-1}$. The second step followed a surface interface reaction kinetics with an activation energy ranging from 93.26 to 99.37 kJ.mol$^{-1}$, depending on the kinetic method used in calculations. In both cases, the kinetic compensation effect was revealed by a linear relation between ln $A$ and $E$. Evidence of cracking of biochar was obtained from the decrease in carbon content following increasing the temperature from 400°C to 500°C.

## 6. Conflicts of interest

The authors have no relevant financial or non-financial interests to disclose.

## 7. Formatting of funding sources

The authors declare that no funds, grants, or other support were received during the preparation of this manuscript.

## 11. References

1. Lazare, S. et al. Jojoba pruning: New practices to rejuvenate the plant, improve yield and reduce alternate bearing. Scientia Horticulturae277, 109793(2021). https://doi.org/10.1016/j.scienta.2020.109793
2. Elsanhoty, R. M., Al-Soqeer, A. & Ramadan, M. F. Effect of detoxification methods on the quality and safety of jojoba (Simmondsia chinensis) meal. Journal of Food Biochemistry41, 1–10 (2017). https://doi.org/10.1111/jfbc.12400
3. Sánchez, M., Avhad, M. R., Marchetti, J. M., Martínez, M. & Aracil, J. Jojoba oil: A state of the art review and future prospects. Energy Conversion and Management129, 293–304 (2016).https://doi.org/10.1016/j.enconman.2016.10.038
4. Wisniak, J. Potential uses of jojoba oil and meal - a review. Industrial Crops and Products3, 43–68 (1994).https://doi.org/10.1016/09266690(94)90077-9
5. Bellirou, A. et al. Extraction of simmondsin and oil in one step from jojoba seeds. Industrial Crops and Products21, 229–233 (2005). https://doi.org/10.1016/j.indcrop.2004.04.007
6. Cokelaere, M. M., Dangreau, H. D., Arnouts, S., Kühn, E. R. & Decuypere, E. M. P. Influence of Pure Simmondsin on the Food Intake in Rats. Journal of Agricultural and Food Chemistry40, 1839–1842 (1992). https://doi.org/10.1021/jf00022a022
7. Wagdy, S. M., Taha, F. S. & Omar, S. S. Influence of reduced phenolics and simmondsins contents on protein quality of defatted jojoba meal. American Journal of Food Technology11, 213–220 (2016). https://doi.org/10.3923/ajft.2016.213.220
8. Chaudhary, V. & Tripathi, R. S. Feeding Deterrence Effects of Defatted Jojoba (Simmondisa chinensis) Meal Against Indian Gerbil, Tatera indica (Hardwicke). Proceedings of the National Academy of Sciences India Section B - Biological Sciences87, 663–670 (2017). https://doi.org/10.1007/s40011-015-0633-7
9. Boven, M. Van, Busson, R., Cokelaere, M., Flo, G. & Decuypere, E. 4-Demethyl simmondsin fromSimmondsia chinensis . 12, 203–208 (2000).10.3923/ajft.2016.213.220. https://doi.org/10.1016/S0926-6690(00)00072-8
10. Zhang, D., Wang, T., Zhi, J., Zheng, Q. & Chen, Q. Utilization of Jujube Biomass to Prepare Biochar for Nitrogen. Materials13, (2020).https://doi.org/10.3390/ma13245594
11. Cui, Y., Wang, W. & Chang, J. Study on the product characteristics of pyrolysis lignin with calcium salt additives. Materials12, (2019).https://doi.org/10.3390/ma12101609
12. Açıkalın, K. Evaluation of orange and potato peels as an energy source: a comprehensive study on their pyrolysis characteristics and kinetics. Biomass Conversion and Biorefinery12, 501–514 (2022).https://doi.org/10.1007/s13399-021-01387-z
13. Pravin Kumar, S. A., Nagarajan, R., Midhun Prasad, K., Anand, B. & Murugavelh, S. Thermogravimetric study and kinetics of banana peel pyrolysis: a comparison of 'model-free' methods. Biofuels13, 129–138 (2022). https://doi.org/10.1080/17597269.2019.1647375
14. Phuakpunk, K., Chalermsinsuwan, B. & Assabumrungrat, S. Comparison of chemical reaction kinetic models for corn cob pyrolysis. Energy Reports6, 168–178 (2020).https://doi.org/10.1016/j.egyr.2020.08.041
15. Mahmood, H., Shakeel, A., Abdullah, A., Khan, M. I. & Moniruzzaman, M. A comparative study on suitability of model-free and model-fitting kinetic methods to non-isothermal degradation of lignocellulosic materials. Polymers13, (2021).https://doi.org/10.3390/polym13152504
16. Tsekos, Chr, et al. "Kinetic Modeling for the Pyrolysis of Biomass Fuels derived from Oil Crops." Proc. Eur. Combust. Meet 1 (2015).http://www.ecm2015.hu/papers/P1-57.pdf.
17. Saeed, S., Ashour, I., Sherif, H. & Ali, M. R. O. Catalytic and noncatalytic fast pyrolysis of jatropha seeds: Experimental measurements and modeling. Egyptian Journal of Chemistry63, 683–702 (2020). 10.21608/ejchem.2019.19911.2201
18. Sharma, R., Sheth, P. N. & Gujrathi, A. M. Kinetic modeling and simulation: Pyrolysis of Jatropha residue de-oiled cake. Renewable Energy86, 554–562 (2016). https://doi.org/10.1016/j.renene.2015.08.066
19. Jin, X. et al. Determination of hemicellulose , cellulose and lignin content using visible and near infrared spectroscopy in Miscanthus

sinensis. Bioresource Technology 241, 603–609 (2017). https://doi.org/10.1016/j.biortech.2017.05.047
20. Van Soest, P. J. & Wine, R. H. Use of detergents in the analysis of fibrous feeds IV. Determination of plant cell-wall constituents. Journal of the Association of Official Analytical Chemists. 58, 50–55 (1967). https://www.scirp.org/(S(lz5mqp453edsnp55rrgjct55))/reference/referencespapers.aspx?referenceid=1496670
21. Collings, G. F., Yokoyama, M. T & Bergen W. G. 1978. Lignin as determined by oxidation with sodium chlorite and a comparison with permanganate lignin. Journal of Dairy Science 61: 1156-1160. (1978). https://www.sciencedirect.com/science/article/pii/S002203027883700X
22. Khawam, A. & Flanagan, D. R. Solid-state kinetic models: Basics and mathematical fundamentals. Journal of Physical Chemistry B110, 17315–17328 (2006). https://doi.org/10.1021/jp062746a
23. Bezgin, F. & Demirelli, K. Synthesis, Characterization and thermal degradation kinetics of photoresponsive graft copolymers. Journal of Thermoplastic Composite Materials29, 1135–1150 (2016).https://doi.org/10.1177/0892705714563114
24. Vyazovkin, S. Kissinger Method in Kinetics of Materials: Things to Beware and Be Aware of. Molecules25, (2020). https://doi.org/10.3390/molecules25122813
25. Mothé, C. G. & De Miranda, I. C. Study of kinetic parameters of thermal decomposition of bagasse and sugarcane straw using Friedman and Ozawa-Flynn-Wall isoconversional methods. Journal of Thermal Analysis and Calorimetry113, 497–505 (2013).https://doi.org/10.1007/s10973-013-3163-7
26. Garn, P. D. An examination of the kinetic compensation effect Journal of Thermal Analysis. 7, 475–478 (1975). https://doi.org/10.1007/BF01911956
27. IR Spectrum Tables and Charts: https://www.sigmaaldrich.com/EG/en/technical-documents/technical-article/analytical-chemistry/photometry-and-reflectometry/ir-spectrum-table.
28. Chandrasekhar, K. and Pandey, S. Co-processing of RDF in Cement Plants. (Springer, Singapore, 2020).
https://doi.org/10.1007/978-981-32-9228-4_19
29. Al-Hamamre, Z. & Rawajfeh, K. M. Investigating the energy value of jojoba as an alternative renewable energy source. International Journal of Green Energy12, 398–404 (2015). https://doi.org/10.1080/15435075.2013.848404
30. Warra, A.A., Wawata I.G. & Umar R.A. Extraction of oil from castor beans using n-hexane World Research Journal of Chemistry. 1 39–41 (2013). https://www.researchgate.net/publication/271075730
31. Sukarni, S. et al. Thermal decomposition behavior of water hyacinth (eichhornia crassipes) under an inert atmosphere. MATEC Web of Conferences 204,(2018).https://doi.org/10.1051/matecconf/201820400010
32. Várhegyi, G., Antal, M. J., Szekely, T. & Szabo, P. Kinetics of the Thermal Decomposition of Cellulose, Hemicellulose, and Sugar Cane Bagasse. Energy and Fuels3, 329–335 (1989).https://doi.org/10.1021/ef00015a012
33. Várhegyi, G., Szabó, P. & Antal, M. J. Reaction Kinetics of the Thermal Decomposition of Cellulose and Hemicellulose in Biomass Materials. Advances in Thermochemical Biomass Conversion 760–770 (1993). https://doi.org/10.1007/978-94-011-1336-6_59
34. Li, H. et al. Mechanisms of metal sorption by biochars: Biochar characteristics and modifications. Chemosphere178, 466–478 (2017). https://doi.org/10.1016/j.chemosphere.2017.03.072
35. Mierzwa-Hersztek, M., Gondek, K., Jewiarz, M. & Dziedzic, K. Assessment of energy parameters of biomass and biochars, leachability of heavy metals and phytotoxicity of their ashes. Journal of Material Cycles and Waste Management21, 786–800 (2019). https://doi.org/10.1007/s10163-019-00832-6
36. Wardani, S., Pranoto & Himawanto, D. A. Kinetic parameters and calorific value of biochar from mahogany (Swietenia macrophylla King) wood pyrolysis with heating rate and final temperature variations. AIP Conference Proceedings2049, (2018). https://doi.org/10.1063/1.5082439